Theory of Slope Flows and Low-Level Jets

by Alan Shapiro
School of Meteorology, University of Oklahoma, Norman, Oklahoma, USA

Croatian–USA Workshop on Mesometeorology, 18–20 June 2012

[Katabatic flow at Mawson's Hut, Antarctica, 1911. Photo by Frank Hurley]

Part 1: Slope flows

- Slope flows are thermally-driven flows associated with slope cooling (katabatic case) or heating (anabatic case). Buoyancy $b=(g/\theta_r)[\theta-\bar{\theta}(z)]$ is mostly < 0 in katabatic flows, and mostly > 0 in anabatic flows.

- Katabatic flows are shallower and more jet-like than anabatic flows.

- Katabatic and anabatic flows are common in mountainous terrain.

- Katabatic flows are common over ice sheets of Greenland and Antarctica (where winds near the coastline can reach hurricane force).

- Peak katabatic winds can be found a few 100s of meters above large glaciers. Only 1 or 2 m to jet maximum over short hills.

- Katabatic winds are hard to model accurately with NWP models because of high resolution needed in the vertical and the **strong static stability** (difficult to parameterize effects of turbulence).

What drives katabatic flows?

Radiative cooling of the slope in a stably-stratified environment creates a potential temperature difference between an air parcel near the slope and the relatively warmer environmental air at same elevation as that parcel:

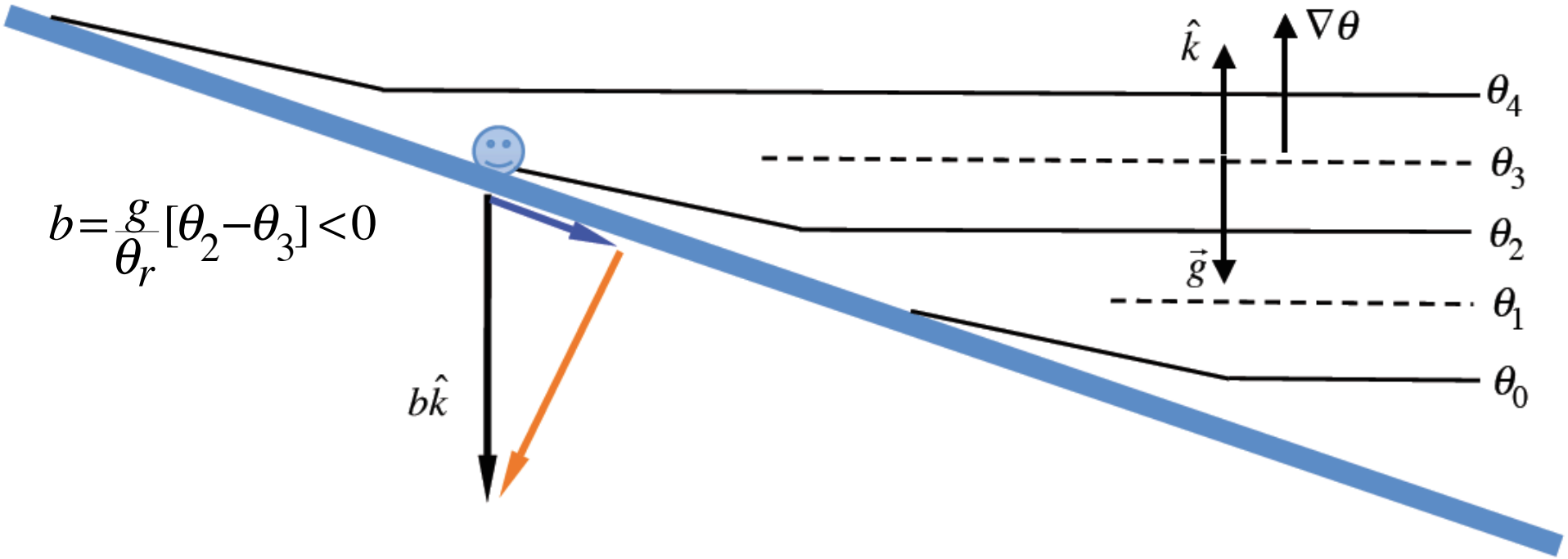

Thus, the parcel experiences a downward buoyancy force. The along-slope component of that force (blue arrow) induces flow down the slope.

What drives anabatic flows?

Radiative heating of the slope in a stably-stratified environment creates a potential temperature difference between an air parcel near the slope and the relatively cooler environmental air at same elevation as that parcel:

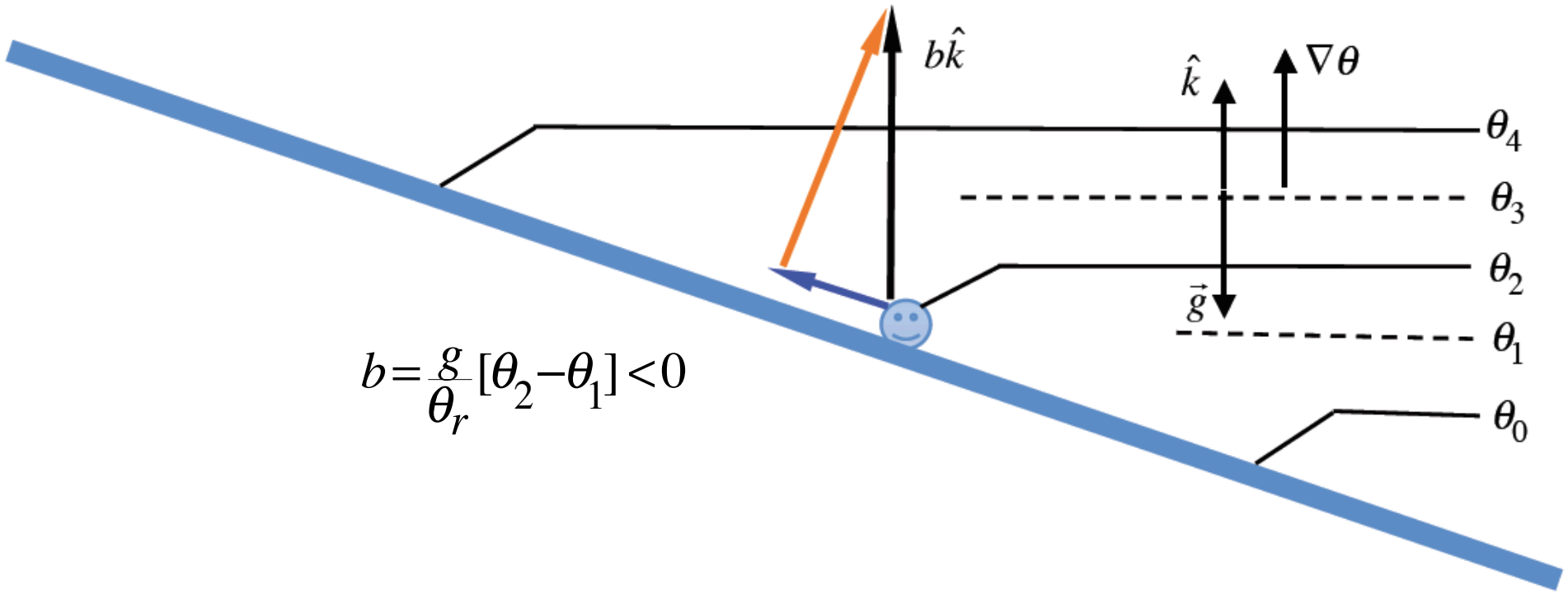

Thus, the parcel experiences an upward buoyancy force. The along-slope component of that force (blue arrow) induces flow up the slope.

A milestone in slope flow theory: Prandtl model (1942)

Prandtl solved the viscous Boussinesq governing equations for slope flow in slope-following coordinates:

X points down slope,
Z points normal slope,
Y points across slope (into page).

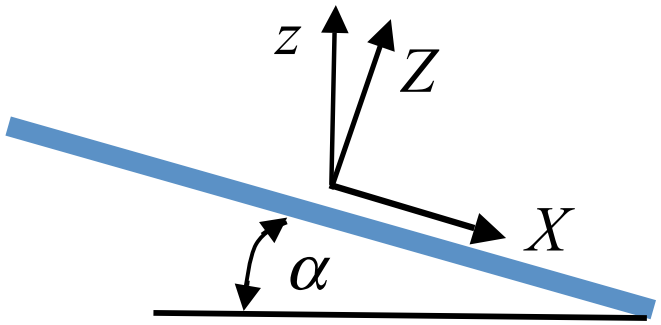

Limitations/restrictions of the theory:

- steady state
- planar slope (α = const) of unbounded extent (no edges)
- constant Brunt-Väisälä frequency $N \equiv \sqrt{(g/\theta_r)\, d\bar{\theta}/dz}$
- eddy viscosity ν and eddy diffusivity κ are constants
- no synoptic-scale forcings (no imposed p.g.f.)
- Coriolis force not included
- surface forcing is spatially constant (independent of X and Y)

Viscous Boussinesq governing equations

X-eqn of motion: $$\frac{\partial u}{\partial t}+\mathbf{v}\cdot\nabla u=-\frac{1}{\rho_r}\frac{\partial p'}{\partial X}+fv-\boldsymbol{b\sin\alpha+\nu\nabla^2 u}, \quad (1)$$

Y-eqn of motion: $$\frac{\partial v}{\partial t}+\mathbf{v}\cdot\nabla v=-\frac{1}{\rho_r}\frac{\partial p'}{\partial Y}-fu+\nu\nabla^2 v, \quad (2)$$

Z-eqn of motion: $$\frac{\partial w}{\partial t}+\mathbf{v}\cdot\nabla w=-\frac{1}{\rho_r}\frac{\partial p'}{\partial Z}+\boldsymbol{b\cos\alpha}+\nu\nabla^2 w, \quad (3)$$

Energy eqn: $$\frac{\partial b}{\partial t}+\mathbf{v}\cdot\nabla b=\boldsymbol{uN^2\sin\alpha}-wN^2\cos\alpha+\boldsymbol{\kappa\nabla^2 b}, \quad (4)$$

Incompressibility: $$\nabla\cdot\mathbf{v}=0. \quad (5)$$

Boundary conditions: no-slip, impermeability, specified surface buoyancy b_0, and all variables vanish far above the slope ($Z\to\infty$).

In view of the limitations/restrictions and the boundary conditions, one can infer that $v=w=0$ everywhere, while u, b, and p' are functions of Z only. So, only a few terms (shown in red) survive. This is a 1D model!

1D Prandtl model equations

X-component equation of motion (1) reduces to a balance between the down-slope component of the buoyancy force and friction:

$$0 = -b\sin\alpha + \nu\frac{d^2u}{dZ^2}. \tag{6}$$

Energy equation (4) reduces to a balance between the down-slope advection of environmental potential temperature and diffusion:

$$0 = u\,N^2\sin\alpha + \kappa\frac{d^2b}{dZ^2}. \tag{7}$$

With variables and parameters suitably redefined, (6) and (7) are identical to the Ekman model equations (Ekman spiral).

Eliminating *b* between (6) and (7) yields a single equation for *u*:

$$\frac{d^4u}{dZ^4} + \left(\frac{N^2\sin^2\alpha}{\nu\kappa}\right)u = 0. \tag{8}$$

Prandtl solution

Applying $u=\sum C_i e^{m_i Z}$ in (8) yields four complex exponents m_i. The boundary conditions pin down four C_i. Get u (and then b) as:

$$u=-\frac{b_0}{N}\sqrt{\kappa/\nu}\, e^{-Z/\delta}\sin(Z/\delta), \qquad b=b_0\, e^{-Z/\delta}\cos(Z/\delta), \tag{9}$$

where $\delta\equiv\sqrt{\frac{2}{N\sin\alpha}}(\nu\kappa)^{1/4}$ is a boundary layer height.

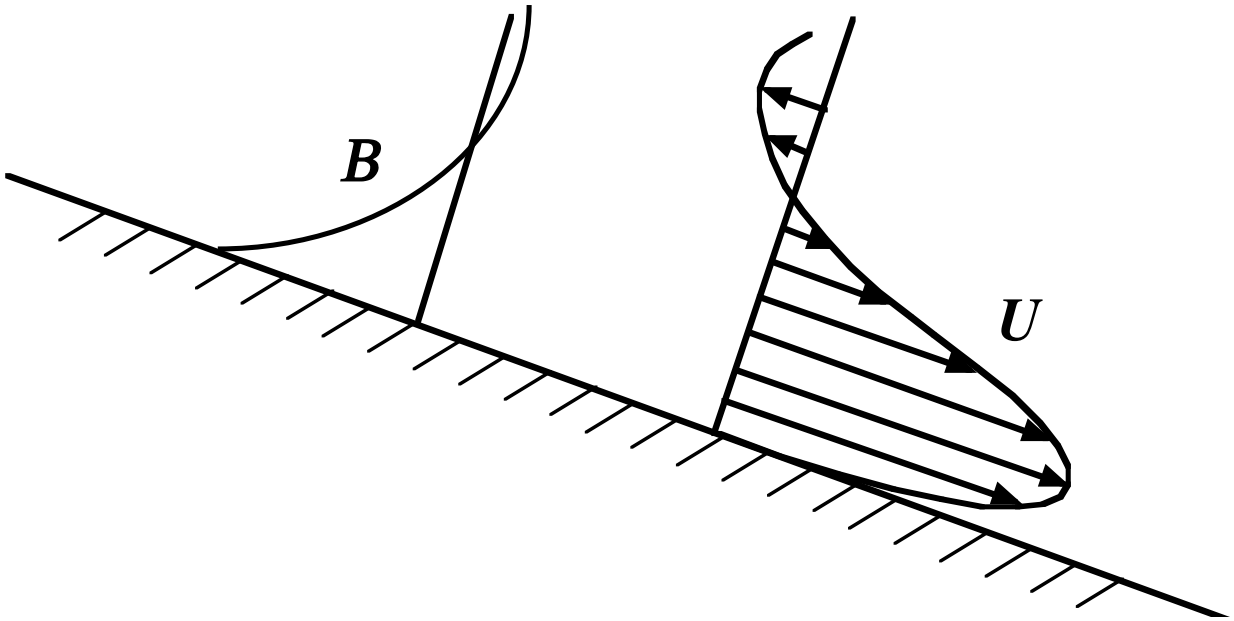

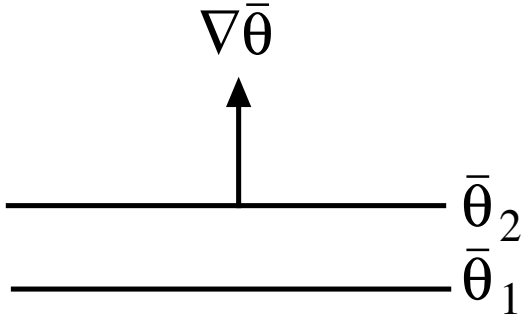

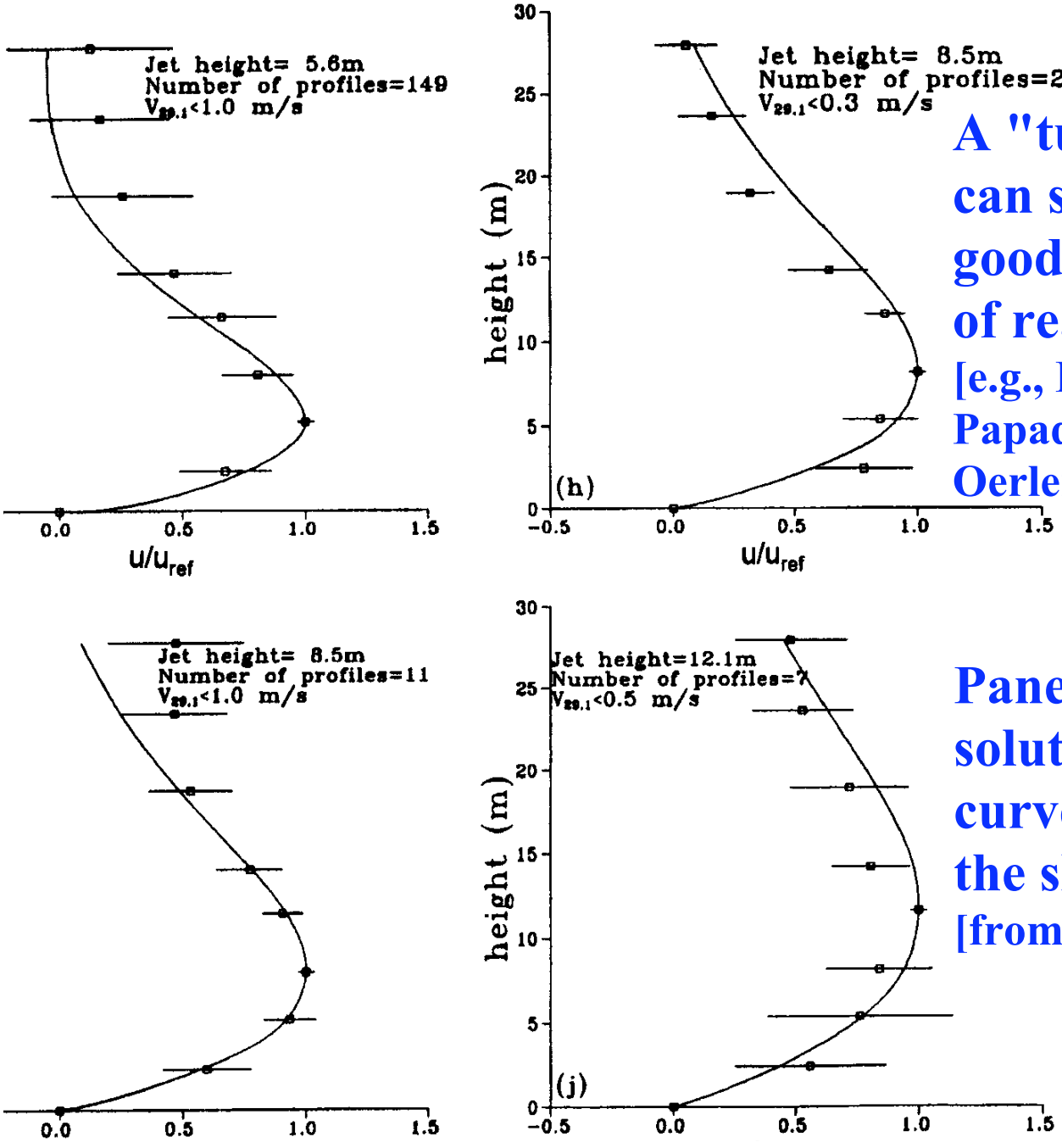

A "tuned" Prandtl solution can sometimes provide a good qualitative fit to data of real katabatic flows
[e.g., Defant 1949; Tyson 1968; Papadopoulos et al. 1997; Oerlemans 1998]

Panels show the Prandtl solution for *u* (solid curves) fit to data from the slope of Mt. Hymettos
[from Papadopoulos et al. 1997]

Extensions of the Prandtl model

Gutman & Malbackov (1964), Lykosov & Gutman (1972), Gutman & Melgarejo (1981), Gutman (1983) considered

- Coriolis force
- external pressure gradient force
- time dependence
- simple but non-constant (eddy) viscosities

Egger (1985), Stiperski et al. (2007), and Shapiro & Fedorovich (2008) further explored the impact of the Coriolis force on flow structure.

Grisogono & Oerlemans (2001, 2002) considered general vertical variations in eddy viscosity via the WKB approximation.

Egger (1981), Kondo (1984), Shapiro & Fedorovich (2007, 2008, 2012), Burkholder et al. (2009) and Axelsen et al. (2010) considered flow response to surface thermal inhomogeneities.

Common thermal inhomogeneities

- Differential cloud cover

- Differential topographic shading (e.g., upper slopes are shaded while lower slopes are sunlit)

- Differential soil moisture (e.g., from variable surface rainfall)

- Isolated patches of snow/ice on a slope

- Variations in snow/ice coverage (e.g., ablation zone of glaciers)

- Variations in vegetation type or coverage

- Variations in land use

An analysis of thermally inhomogeneous katabatic flow

Consider a top-hat profile of buoyancy on a planar slope – the simplest scenario of surface thermal inhomogeneity [Egger 1981; Kondo 1984; Burkholder et al. 2009; Shapiro & Fedorovich 2012].

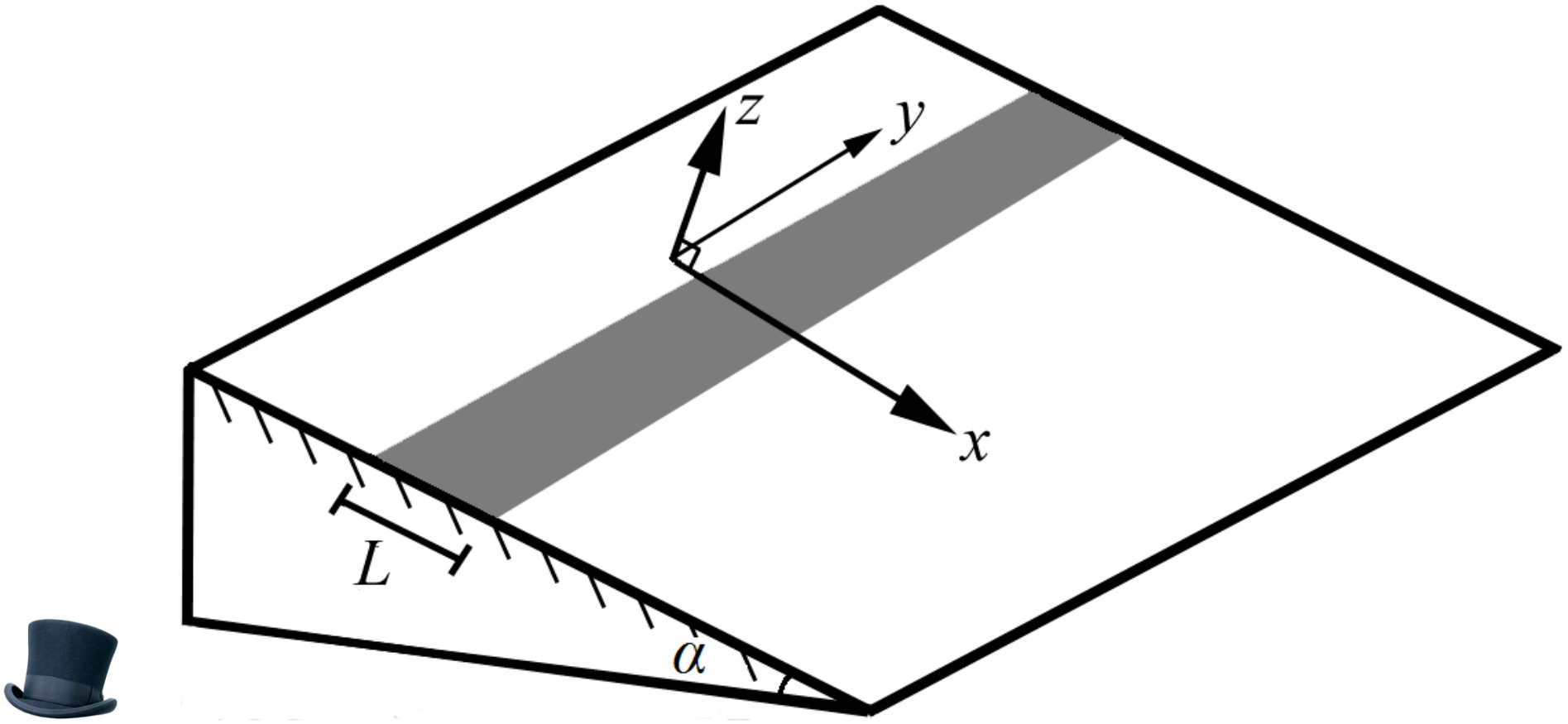

Model assumptions/restrictions

- "Local" katabatic flow – no ambient wind or synoptic-scale p.g.f.
- Steady state
- No Coriolis force
- Linearized Boussinesq dynamics
- Boundary-layer approximation ($\partial^2 U/\partial X^2 << \partial^2 U/\partial Z^2$)
- Quasi-hydrostatic
- Surface cooling varies down the slope (X) but not across the slope (Y). This is a 2D problem.
- Constant ν, κ, and N.

Linearized boundary-layer equations

X-eqn of motion: $$0 = -\frac{\partial \Pi}{\partial X} - B\sin\alpha + \nu\frac{\partial^2 U}{\partial Z^2}\,, \qquad (10)$$

Z-eqn of motion: $$0 = -\frac{\partial \Pi}{\partial Z} + B\cos\alpha, \qquad (11)$$

Energy equation: $$0 = UN^2\sin\alpha - WN^2\cos\alpha + \kappa\frac{\partial^2 B}{\partial Z^2}, \qquad (12)$$

Incompressibility: $$\frac{\partial U}{\partial X} + \frac{\partial W}{\partial Z} = 0\,. \qquad (13)$$

$\Pi \equiv (P - P_\infty)/\rho_r$ is normalized pressure perturbation

$B \equiv g(\Theta - \Theta_\infty)/\Theta_r$ is buoyancy; Θ_∞ is environmental potential temperature

Blue terms were 0 in the Prandtl model. They arise here from 2D effects: convergence, slope-normal motion (W) and advection of Θ_∞ by W. Red terms were in the Prandtl model but were not needed to get U or B.

Non-dimensional variables

Remove as many parameters as possible from the problem by introducing:

$$x \equiv \frac{X}{X_s}, \quad z \equiv \frac{Z}{Z_s}, \quad u \equiv \frac{U}{U_s}, \quad w \equiv \frac{W}{W_s}, \quad \pi \equiv \frac{\Pi}{\Pi_s}, \quad b \equiv \frac{B}{B_s}, \quad (14)$$

where

$$Z_s \equiv \frac{(\nu\kappa)^{1/4}}{(N\sin\alpha)^{1/2}}, \qquad X_s \equiv \frac{(\nu\kappa)^{1/4}\cos\alpha}{N^{1/2}\sin^{3/2}\alpha}, \qquad U_s \equiv \frac{B_s}{N}\left(\frac{\kappa}{\nu}\right)^{1/2},$$

$$W_s \equiv \frac{B_s}{N}\left(\frac{\kappa}{\nu}\right)^{1/2}\frac{\sin\alpha}{\cos\alpha}, \qquad \Pi_s \equiv \frac{B_s(\nu\kappa)^{1/4}\cos\alpha}{(N\sin\alpha)^{1/2}},$$

$$B_s \equiv \begin{cases} \max\limits_{X\in(-\infty,\infty)} \left|B(X,0)\right|, & \text{(if buoyancy is specified),} \\ \max\limits_{X\in(-\infty,\infty)} \left|Z_s\dfrac{\partial B}{\partial Z}(X,0)\right|, & \text{(if buoyancy flux is specified).} \end{cases}$$

Non-dimensional problem

$$0 = -\frac{\partial \pi}{\partial x} - b + \frac{\partial^2 u}{\partial z^2}, \tag{15}$$

$$0 = -\frac{\partial \pi}{\partial z} + b, \tag{16}$$

$$0 = u - w + \frac{\partial^2 b}{\partial z^2}, \tag{17}$$

$$\frac{\partial u}{\partial x} + \frac{\partial w}{\partial z} = 0. \tag{18}$$

Boundary condition for top-hat buoyancy: $b(x,0) = \begin{cases} -1, & |x| \le l, \\ 0, & |x| > l. \end{cases}$ (19)

Thus, a flow driven by a top-hat forcing (cold strip) is fully characterized by a single parameter, the non-dimensional strip width:

$$l \equiv \frac{L}{X_s} = L\,\frac{N^{1/2}\sin^{3/2}\alpha}{(\nu\kappa)^{1/4}\cos\alpha}. \tag{20}$$

Reduction to a single ODE

Taking $\partial/\partial z(5) - \partial/\partial x(6)$ eliminates π and yields the vorticity equation:

$$0 = \underbrace{-\partial b/\partial x}_{\text{Baroclinic generation}} \underbrace{- \partial b/\partial z}_{} + \underbrace{\partial^2\eta/\partial z^2}_{\text{Diffusion of vorticity } \eta=\partial u/\partial z}. \qquad (21)$$

Introduce the streamfunction ψ defined by $u=\partial\psi/\partial z$, $w=-\partial\psi/\partial x$. The energy and vorticity equations then combine to form:

$$\frac{\partial^2\psi}{\partial x^2} + 2\frac{\partial^2\psi}{\partial x\partial z} + \frac{\partial^2\psi}{\partial z^2} + \frac{\partial^6\psi}{\partial z^6} = 0. \qquad (22)$$

Taking the Fourier Transform (FT) of (12) yields the ODE

$$\frac{d^6\hat{\psi}}{dz^6} + \frac{d^2\hat{\psi}}{dz^2} + 2ik\frac{d\hat{\psi}}{dz} - k^2\hat{\psi} = 0, \qquad (23)$$

where $\hat{\psi}$ is the FT of ψ.

Solving the ODE

Apply $\hat{\psi} \sim \exp(mz)$ in (23), get:

$$m^6 = -(ik + m)^2 . \tag{24}$$

Taking the square root of (24) yields the cubic equation (well 2 equations),

$$m^3 = \pm(im - k) . \tag{25}$$

Solve (25) but reject solutions with $\mathrm{Re}(m) > 0$ to avoid blow-up of $\hat{\psi}$ (and ψ) far above the slope. The general solution for $\hat{\psi}$ is then:

$$\hat{\psi} = n_1 \exp(m_1 z) + n_2 \exp(m_2 z) + n_3 \exp(m_3 z). \tag{26}$$

Get n_1, n_2, n_3 from boundary conditions. Get ψ from inverse FT of (26).

Top-hat results for large *l*

Contour plots of ψ and b show that for large l, all flow structures become independent of l – one solution fits all. Results are shown here for $l = 40$.

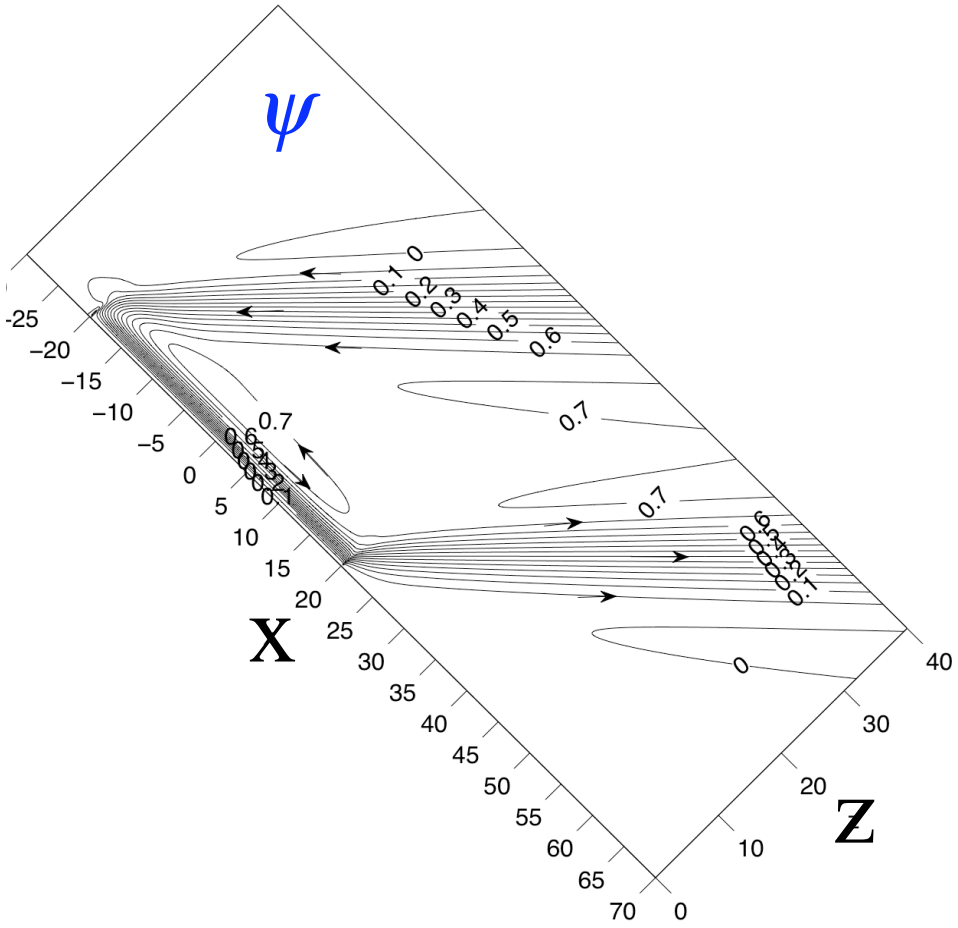

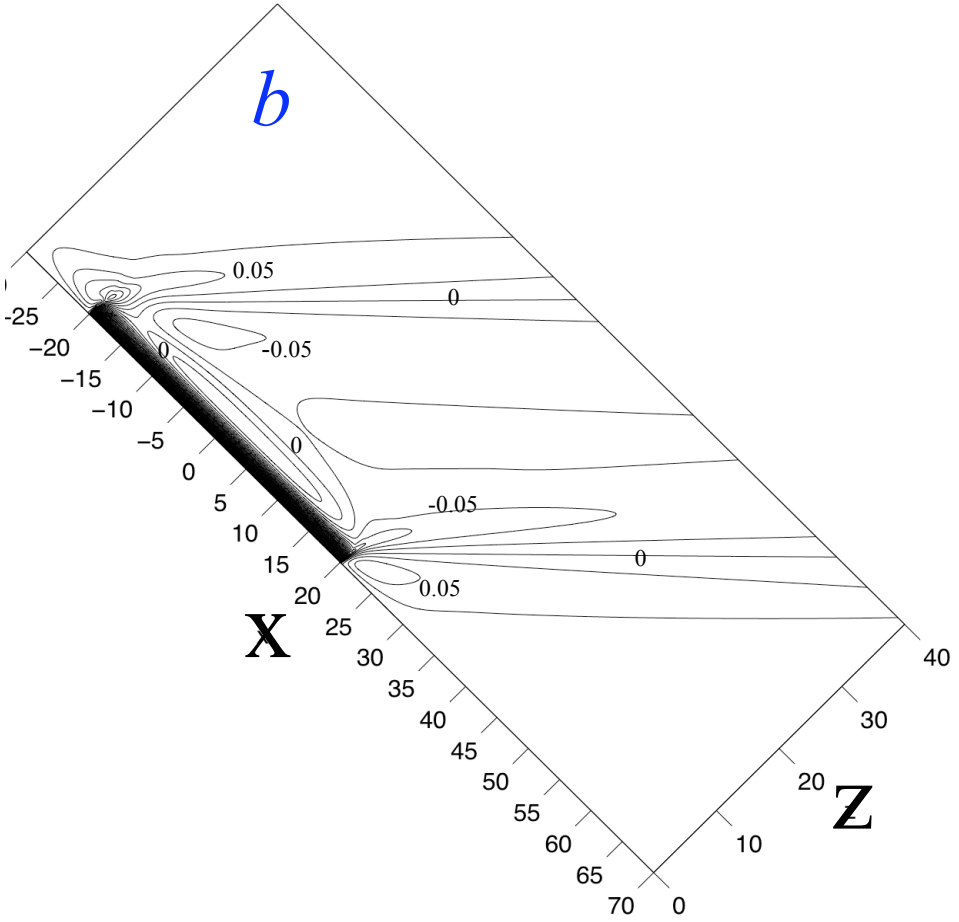

Profiles of u and b near the center of cold strip ($x = 0$)

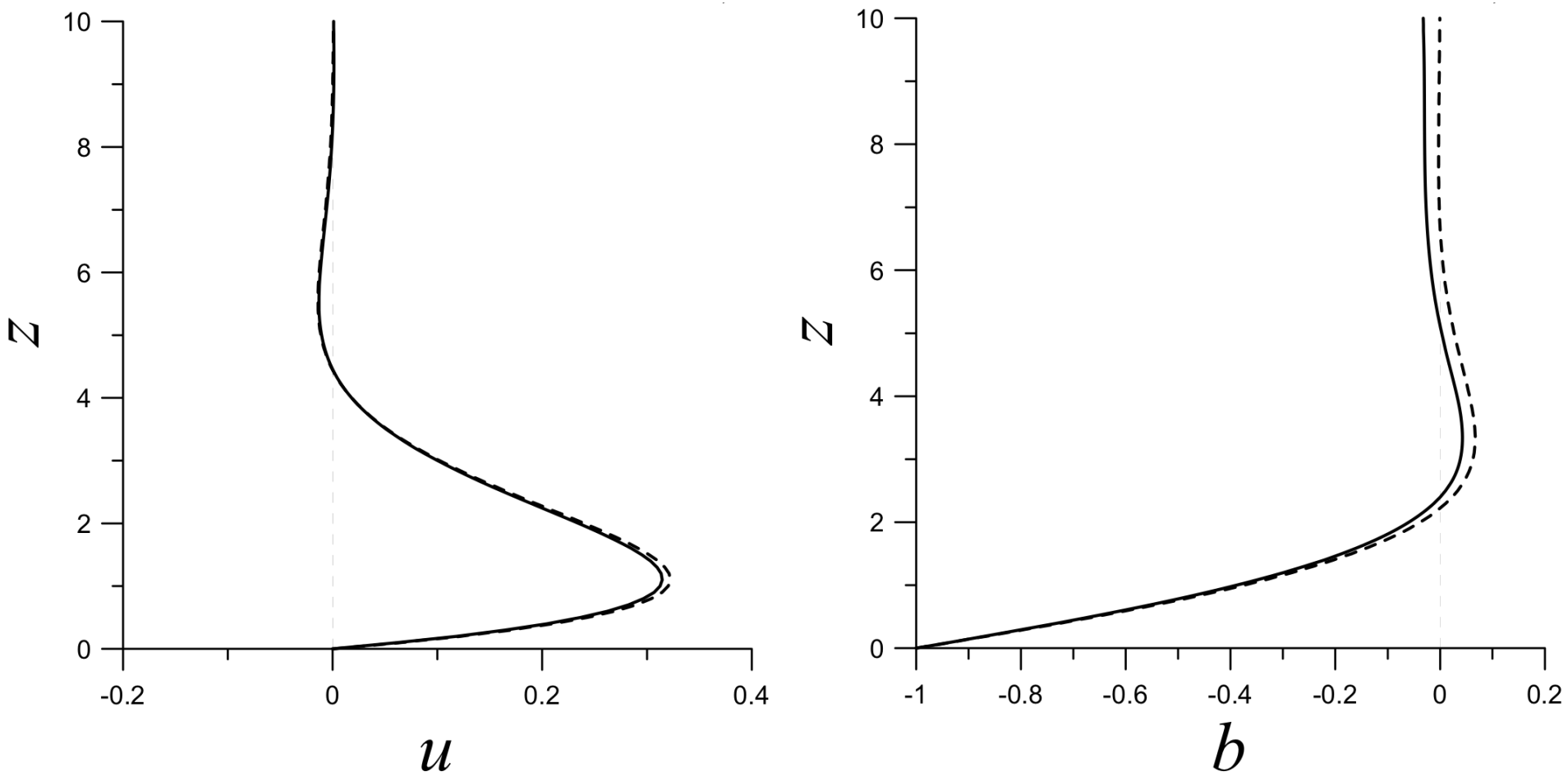

——————— Solid lines depict solution from the Fourier analysis.

- - - - - - - - Dashed lines depict Prandtl solution.

Close-up view of flow near up-slope edge of cold strip

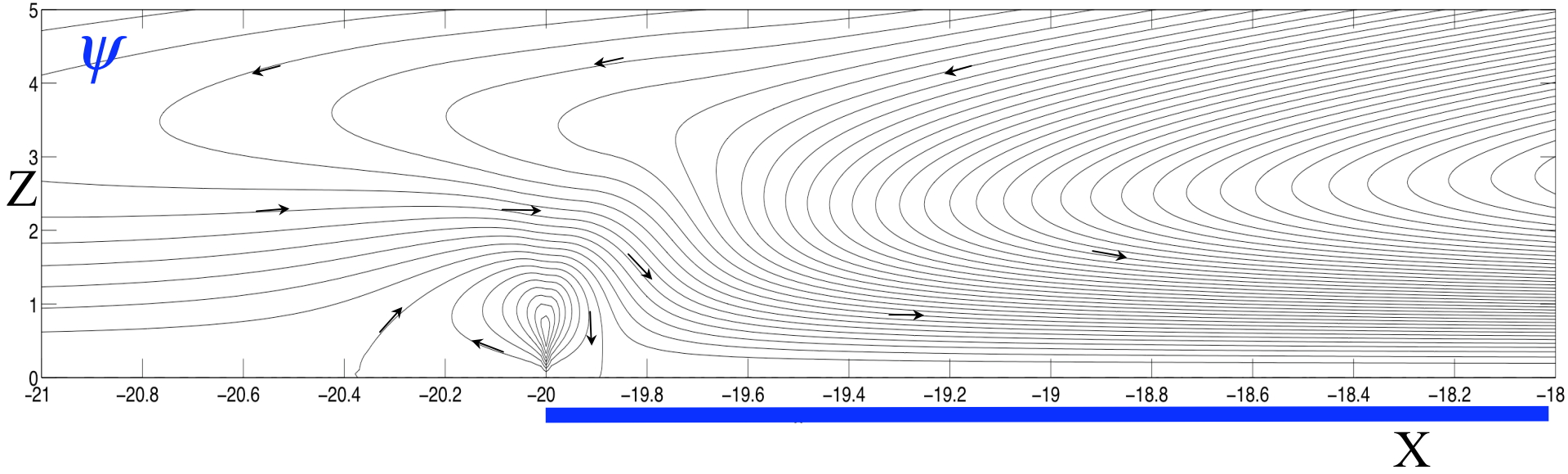

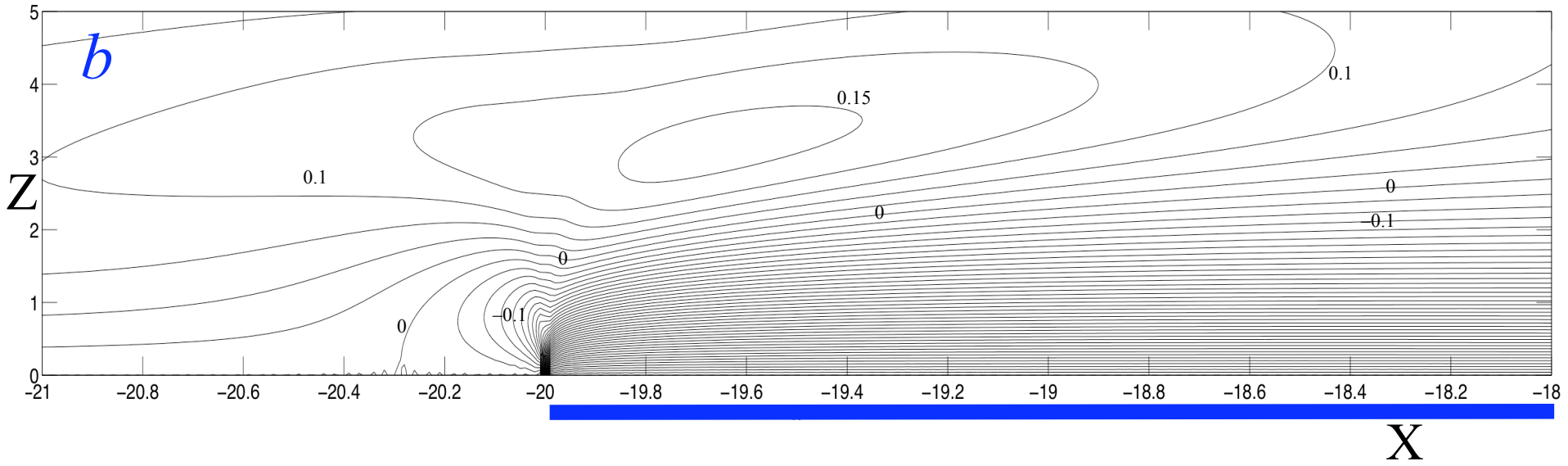

Direct numerical simulation (DNS)

The nonlinear initial value problem for a suddenly imposed top-hat cold strip was solved via DNS. Experiments were performed to:

- verify analytical work (weak thermal disturbance)

- explore non-linear aspects of the flow (stronger disturbance, $\Delta T = 3\,K$)

- examine transient solution leading to the steady state

DNS code was a parallel version of code used by Fedorovich et al. (2001), Shapiro & Fedorovich (2004, 2006, 2007), and Burkholder et al. (2009).

Physical parameters chosen to coincide with the $l = 40$ experiment:

$\alpha = 15^{\circ}$, $N = 0.01\ \mathrm{s}^{-1}$, $\nu = \kappa = 1\ \mathrm{m}^2\mathrm{s}^{-1}$, $L = 2.8\ \mathrm{km}$ ($l = 40$)

Ψ and b at $t \sim 81$ min for $l = 40$ case

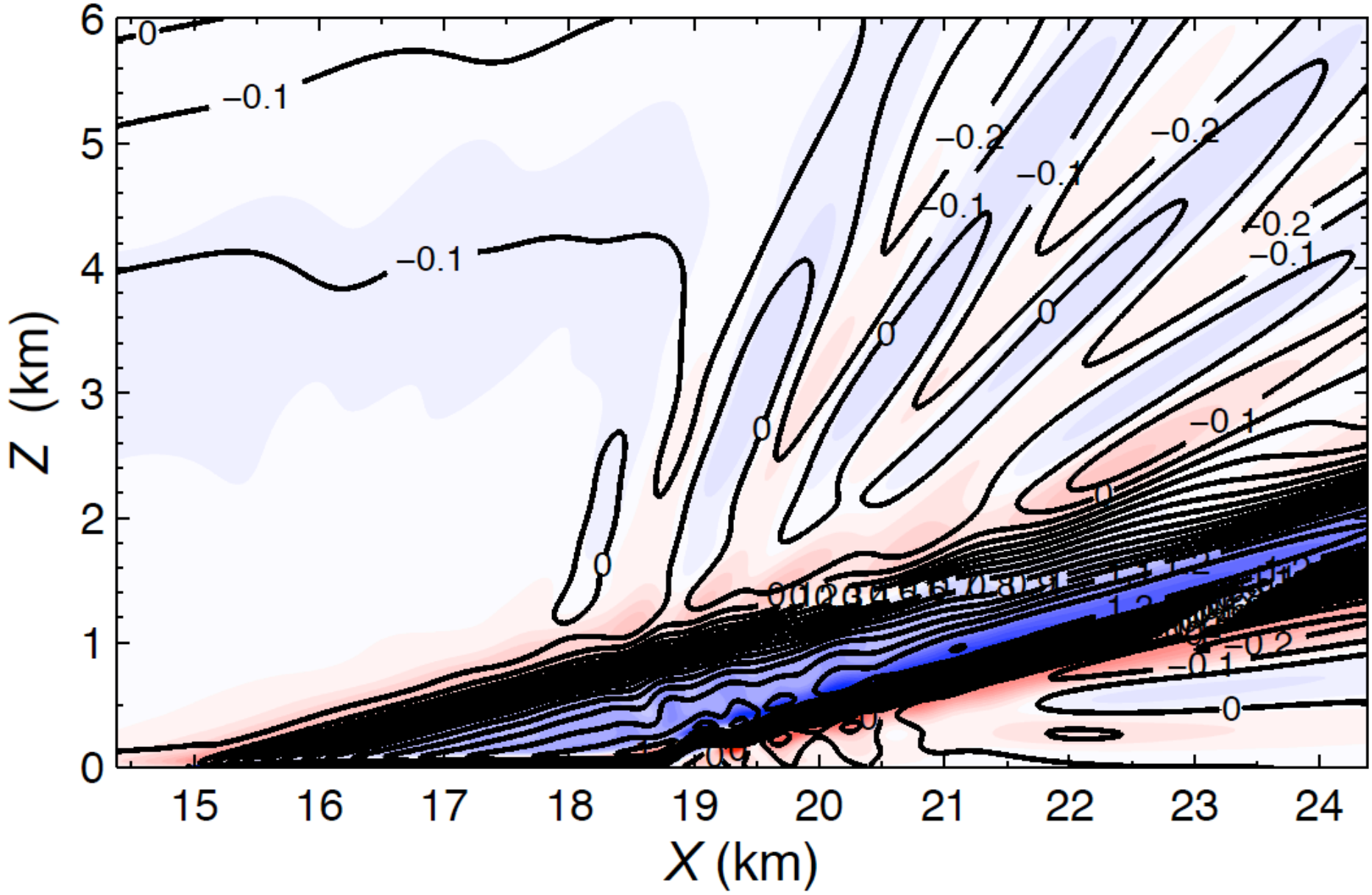

Zoomed-in view at $t = 81$ min

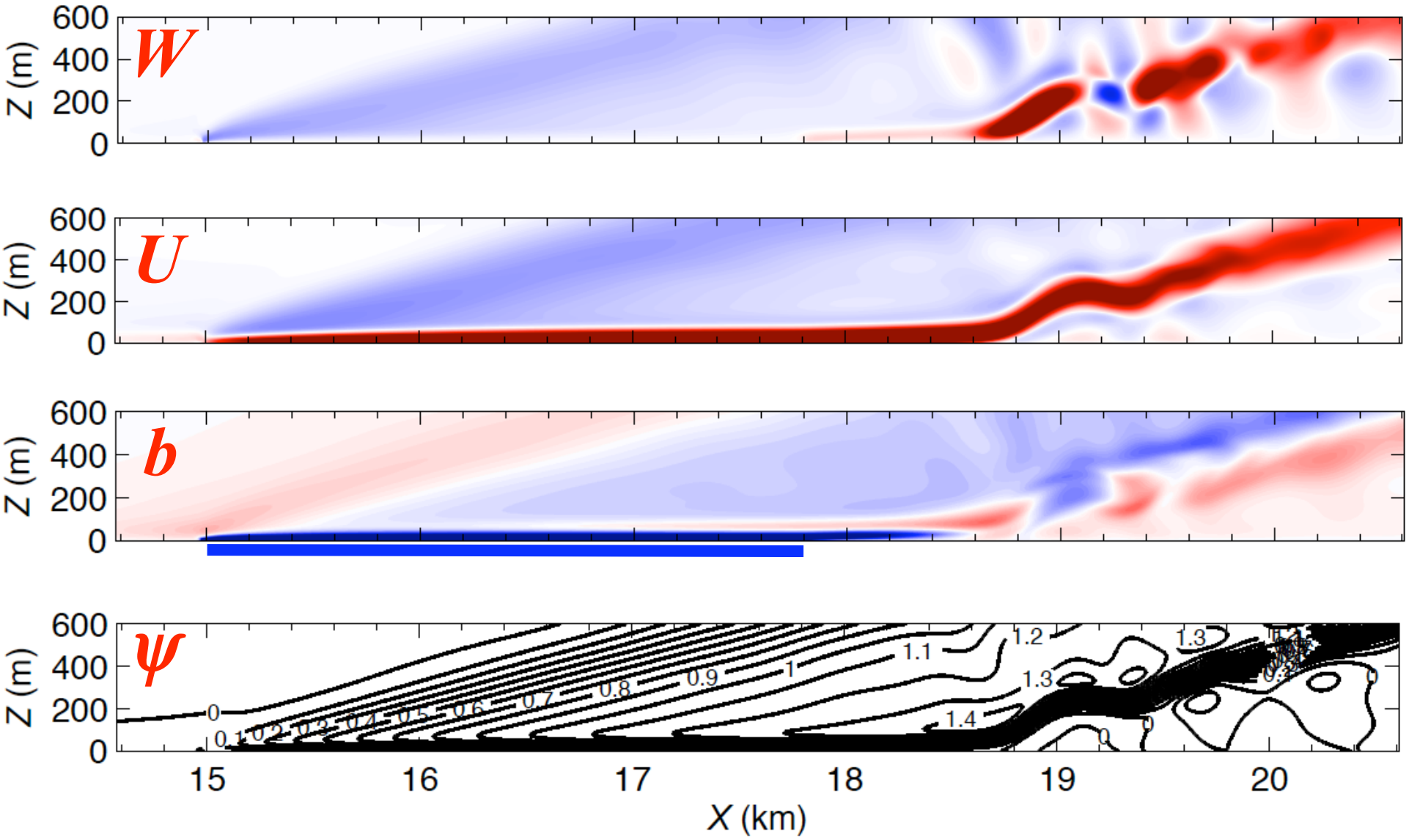

Part 2: Low-level jets

[Photo by Marven Bredel http://www.flickr.com/photos/marvinok/5394411086/in/photostream/]

Characteristics of nocturnal low-level jets

- Low-level jets (LLJs) are a warm-season boundary-layer phenomenon common to the Great Plains of the US and other places worldwide

- LLJs begin to develop around sunset, under dry cloud-free conditions

- LLJs reach peak intensity in the early morning (e.g. 2 a.m. LST) then dissipate shortly after dawn, with onset of convective mixing

- Peak jet winds are supergeostrophic. Strongest jets can have peak winds several 100s of percent stronger than geostrophic.

- Peak winds typically found at $z<1$ km (often <500 m or even <200 m)

- Wind hodograph rotates anticyclonically with time (for fixed z)

- Over the Great Plains of the US, LLJs are often associated with strong southerly geostrophic winds

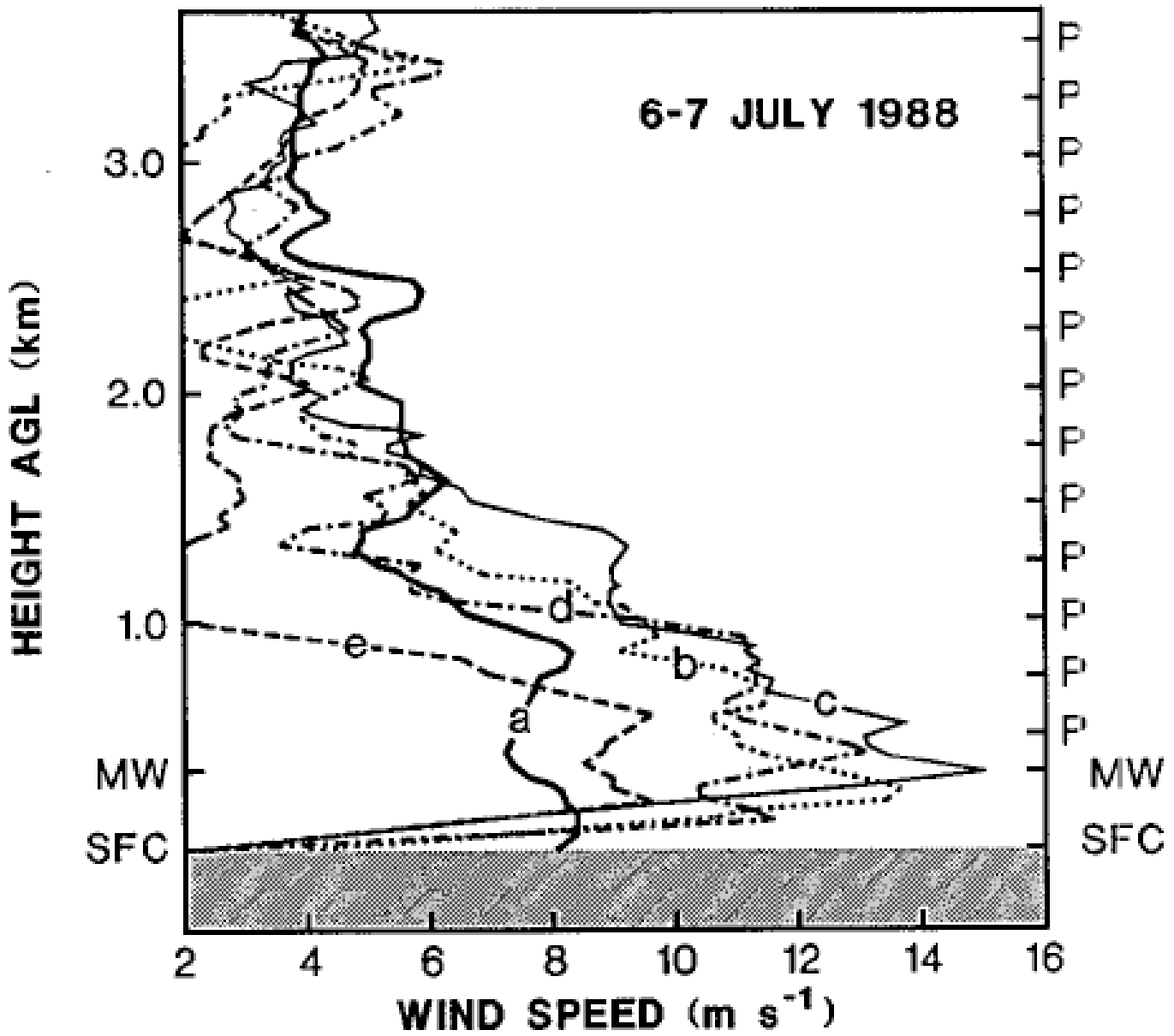

Wind speed versus height at (a) 2331 UTC 6 July, (b) 0229 UTC 7 July, (c) 0535 UTC 7 July, (d) 0830 UTC 7 July, and (e) 1127 UTC 7 July [From Stensrud et al. 1990]

Impacts of LLJs on weather and regional climate

- LLJs provide dynamical and thermodynamical support for deep convection and heavy rain events

- LLJs provide energy to the wind-energy industry but their shear and turbulence can damage wind-turbine rotors

- LLJs transport pollutants hundreds of miles over the course of a night

- LLJs transport agricultural pests and disease carriers (insects, fungi)

- Momentum transport in their decay stage promotes wildfire blow-up

- Strong wind shear in LLJs is a hazard for small aircraft during takeoff or landing

Blackadar (1957) inertial oscillation theory for LLJs

Daytime

Vigorous dry-convective mixing in the boundary layer. Get a 3-way balance between pressure gradient force (p.g.f.), Coriolis force, and friction (turbulent stresses).

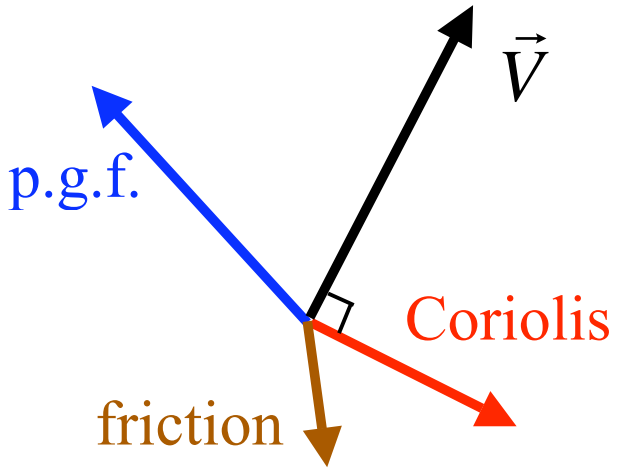

Sunset

Rapid stabilization of the boundary layer. Dry-convective mixing ceases. Turbulent stresses shut down. Air parcels suddenly accelerate (in direction opposite daytime friction force).

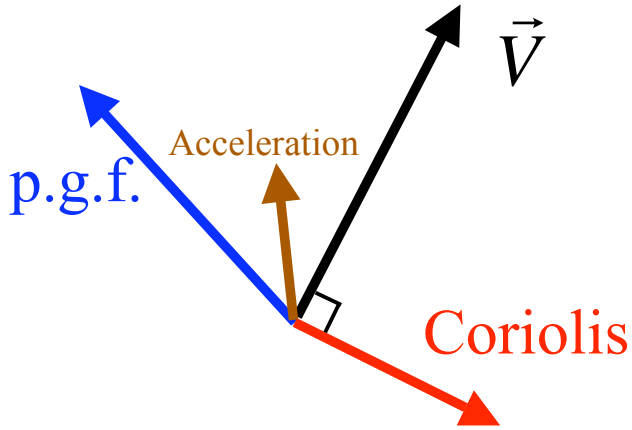

Nighttime

Coriolis force deflects the flow to the right.
Get an anticyclonic inertial oscillation.

Schematic of a Blackadar inertial oscillation

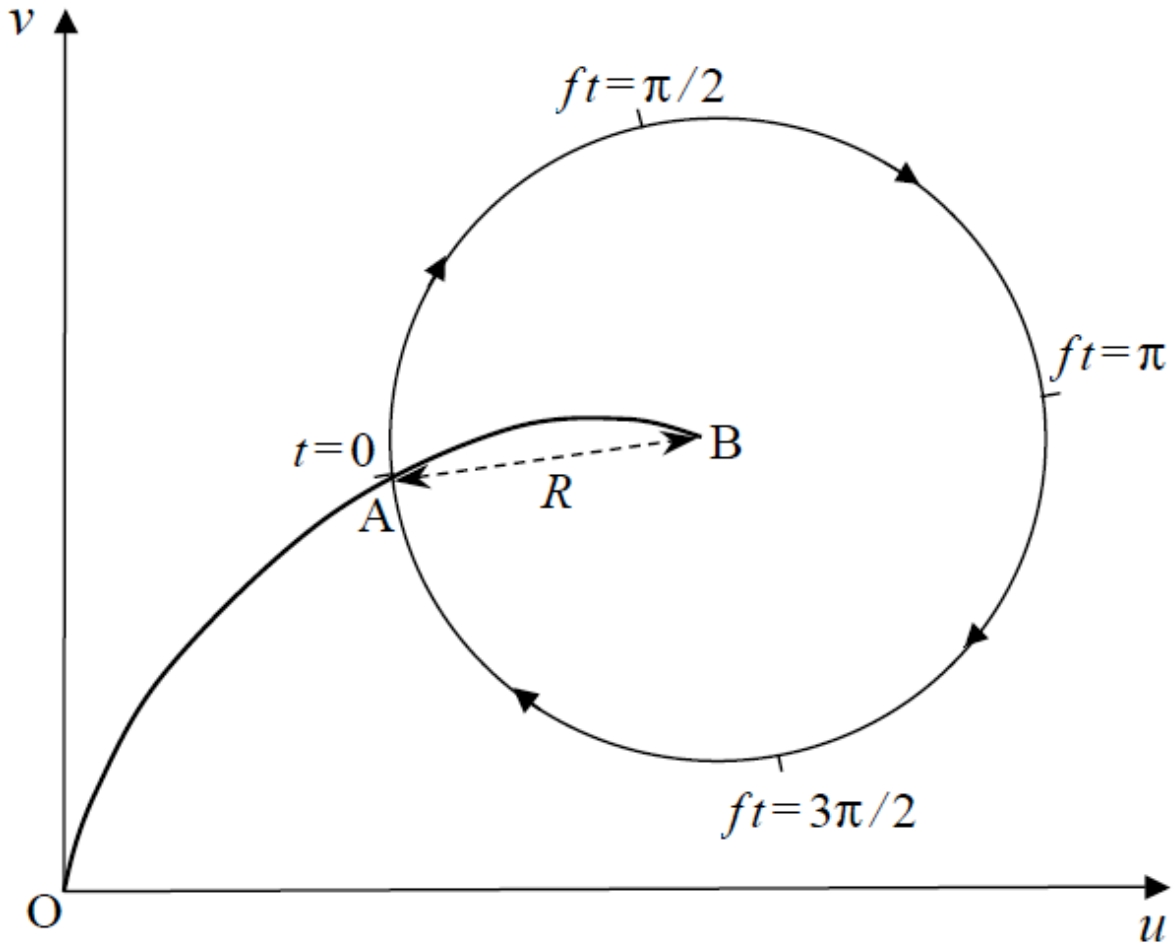

Curve OAB is daytime wind hodograph. Point B is the geostrophic wind at top of the boundary layer. The oscillation amplitude (radius R) is equal to the initial (sunset) ageostrophic wind speed.

Maximum LLJ wind speed in the Blackadar scenario

The actual wind is part geostrophic wind and part not-geostrophic wind:

$$\vec{V} = \vec{V}_{\text{geostrophic}} + \vec{V}_{\text{ageostrophic}}$$

At the ground (point O on hodograph diagram) where the wind is 0 (no-slip), the ageostrophic wind is equal and opposite to the geostrophic wind .

Thus, the largest possible value of the ageostrophic wind speed (and therefore largest possible *R*) is the geostrophic wind speed.

Thus, the largest LLJ wind speed possible in the Blackadar scenario is twice the geostrophic wind speed.

Limitations of the Blackadar theory

1. Cannot explain how peak winds in some LLJs exceed geostrophic values by several 100%.
2. Cannot explain the geographical preference of Great Plains LLJs.

LLJ frequency over the Great Plains of the US (from Bonner 1968)

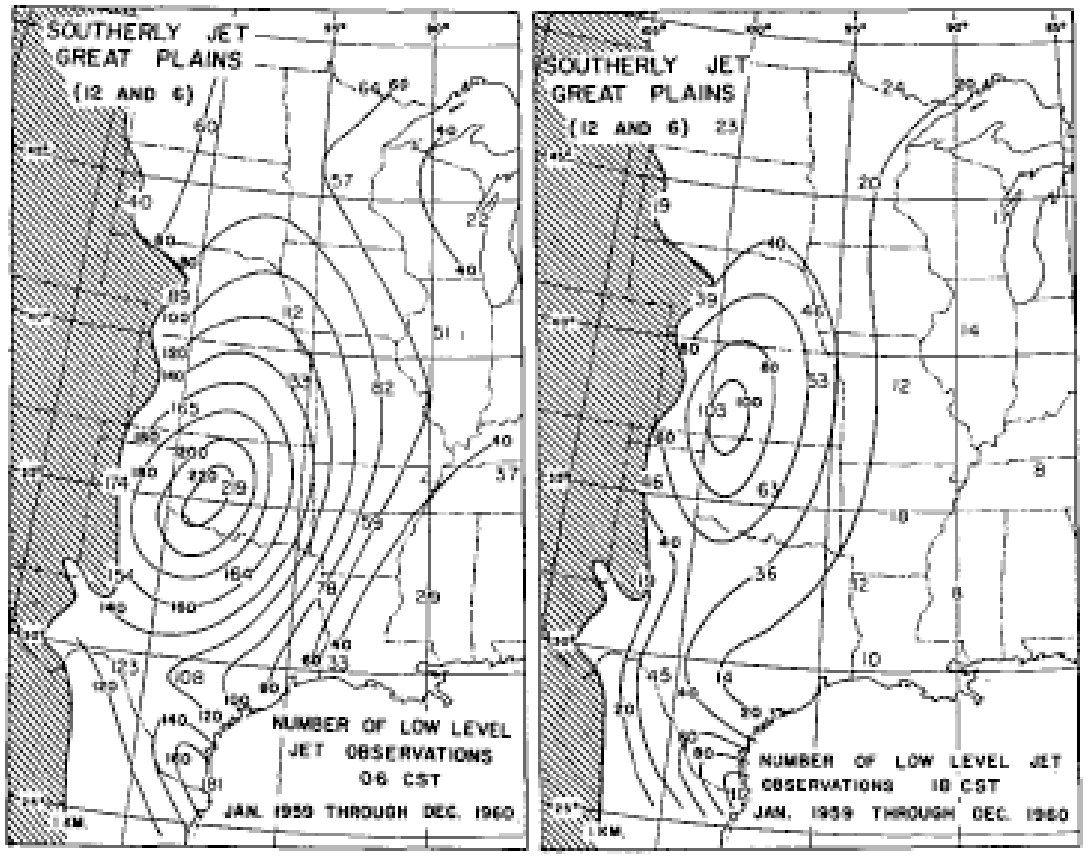

FIGURE 10.—Numbers of Criterion 1 "southerly jet" observations at 06 CST (left) and 18 CST (right). Two years of data.

3. Daytime winds vary with *z* less than in Blackadar schematic.

Daytime winds in Blackadar schematic (his Fig. 10):

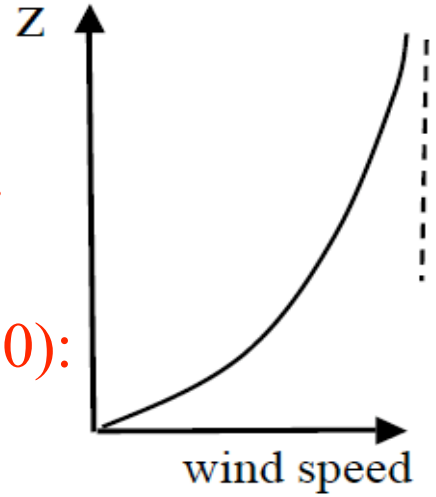

Peak winds in the ensuing inertial oscillation:

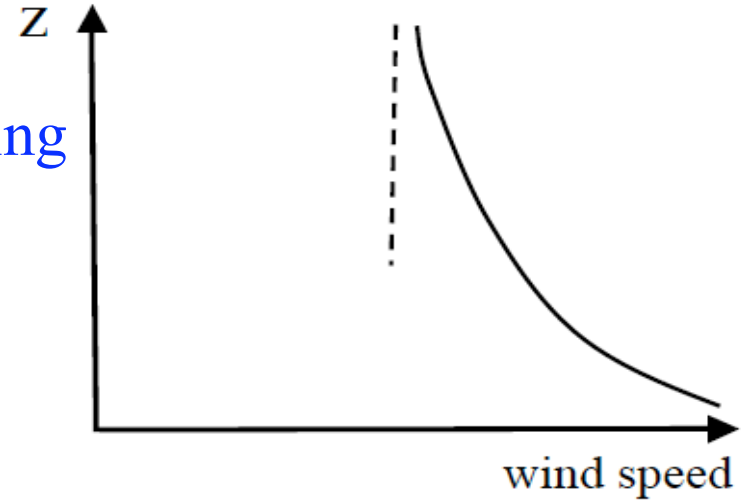

More realistic daytime winds:

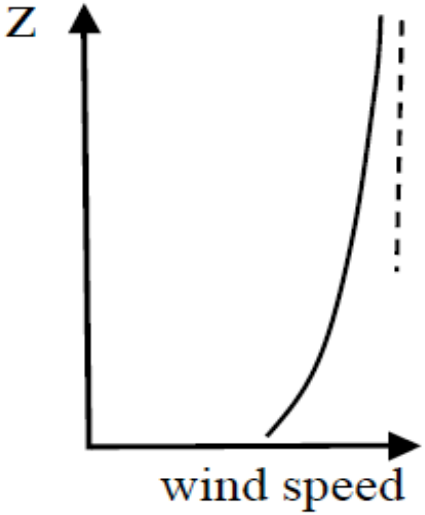

Peak winds in the ensuing inertial oscillation:

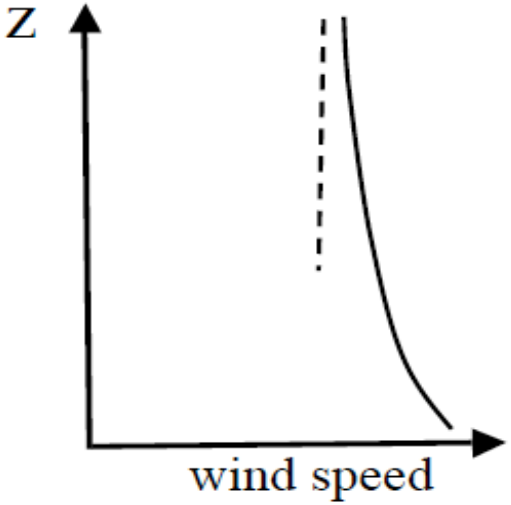

Given realistic daytime wind profiles, the Blackadar inertia oscillation theory would yield weak and not-very-jet-like LLJs.

How does terrain slope affect LLJ formation?

How large is the slope in regions where the LLJ is most prevalent?

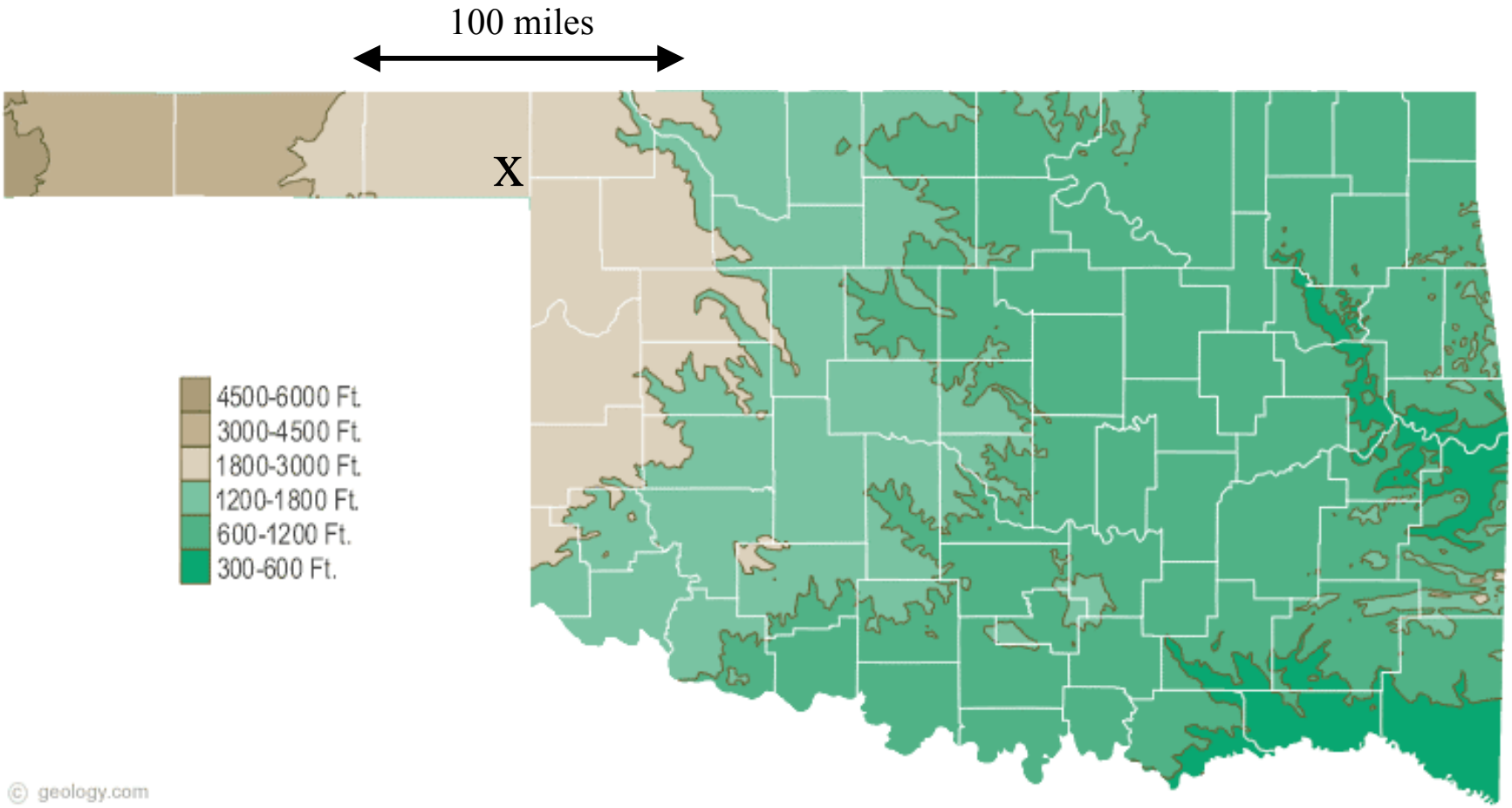

Slope of terrain near Slapout, OK ≈ (3000 ft - 1800 ft)/100 miles ≈ 0.0023 (≈0.15°). Pretty wimpy!

Holton (1967) sloping boundary layer theory for LLJs

Holton (1967) solved the viscous equations of motion and energy for a stably-stratified sloping boundary layer.

Attention restricted to constant southerly geostrophic wind, and an periodic (monochromatic, T = 24 hr) volumetric radiative forcing. Eddy viscosity was constant in time – unlike the Blackadar scenario.

A diurnal wind oscillation was induced, but the results did not correctly reproduce the observed phase of the diurnal oscillations, and arguably the flow was not as jet-like as in observations.

Bonner & Paegle (1970) sloping boundary layer theory for LLJs

Bonner & Paegle (1970) considered time-varying eddy viscosity and geostrophic wind.

Periodicity of the geostrophic wind was ascribed to diurnal temperature cycle over gently sloping terrain but the analysis did not explicitly take terrain into account.

Results were in reasonable agreement with observations, but amplitude of the oscillation was very sensitive to the magnitude of the geostrophic wind, choice of viscosity, and phase difference between the viscosity and the geostrophic wind.

Shapiro & Fedorovich (2009) sloping boundary layer theory for LLJs

Shapiro & Fedorovich (2009) examined effects of terrain slope, thermal boundary layer structure, environmental stratification and synoptic-scale p.g.f. on LLJ evolution.

Considered a very simple framework: extended the inviscid, 1D Blackadar theory to include slope angle and a coupling between the equations of motion and thermal energy (stratification effects).

Treated LLJ as a response to the release of the frictional constraint near sunset, but considered the nature of the force(s) suddenly left unopposed to be a combination of the p.g.f. and buoyancy.

We will now examine this theory in more detail.

Problem formulation

Consider the development of a LLJ over a planar slope of infinite extent (no edges) having slope angle α. Work in slope-following coordinates.

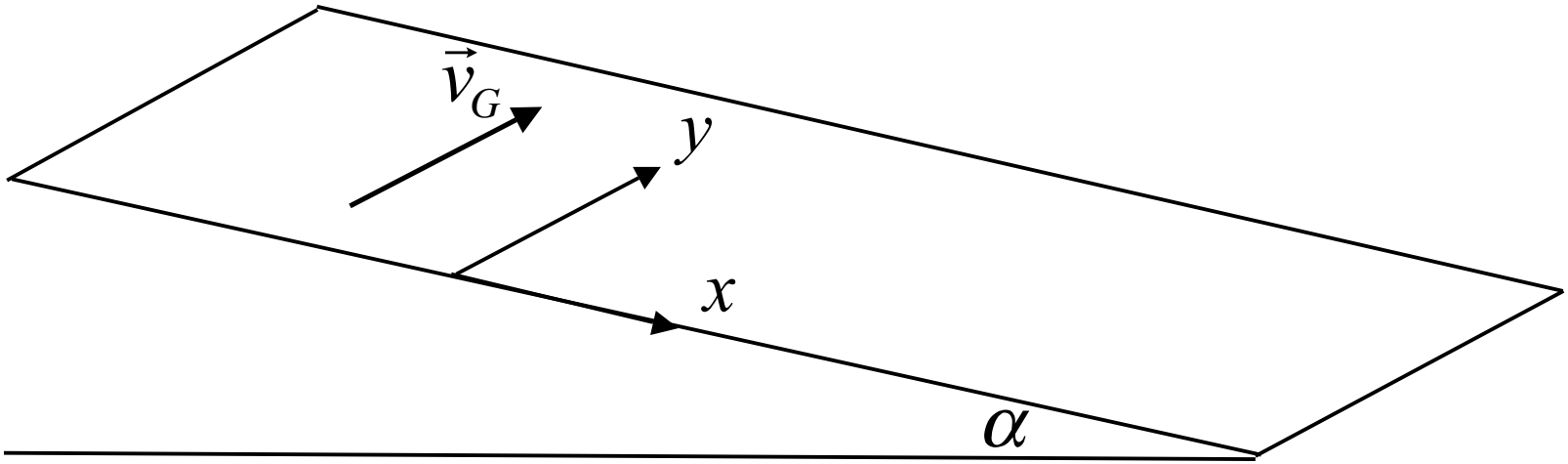

Restrict attention to (typical) case where synoptic-scale p.g.f. points west, so geostrophic wind is southerly ($v_G > 0$), and treat f, v_G, N as constant. These restrictions were also considered by Holton (1967).

Governing equations

$$\frac{du}{dt} = -b\sin\alpha + fv - fv_G, \quad (1)$$

$$\frac{dv}{dt} = -fu, \quad (2)$$

$$\frac{db}{dt} = uN^2\sin\alpha, \quad (3)$$

u, v are down- and cross-slope velocity components, respectively,

$b \equiv g(\theta - \theta_e)/\theta_r$, where θ_e is free-atmosphere potential temperature,

$N \equiv \sqrt{(g/\theta_r)d\theta_e/dz}$ is Brunt-Väisälä frequency,

v_G is geostrophic wind,

f is Coriolis parameter.

Terms in blue not accounted for in Blackadar theory. From (3): upslope flow ($u < 0$) cools parcels while downslope flow ($u > 0$) warms parcels.

Non-dimensionalization

Remove as many parameters as possible from the problem by introducing the non-dimensional variables,

$$U \equiv \frac{u}{v_G}, \quad V \equiv \frac{v}{v_G}, \quad B \equiv \frac{b\sin\alpha}{f v_G}, \quad T \equiv ft, \tag{4}$$

and the parameters,

$$\mathrm{Bu} \equiv \frac{N^2 \sin^2\alpha}{f^2}, \quad \text{(slope Burger number)}, \tag{5}$$

$$\Omega \equiv \sqrt{1+\mathrm{Bu}}, \tag{6}$$

Note that stronger stratification (larger N^2) is associated with larger Bu and larger Ω.

Analytical solution of (1)-(3)

The solutions for U, V, and B, expressed as deviations from their initial values are:

$$U(T)-U_0 = U_0\left(\cos\Omega T-1\right) + \frac{1}{\Omega}\left(-B_0+V_0-1\right)\sin\Omega T, \qquad (7)$$

$$V(T)-V_0 = -\frac{U_0}{\Omega}\sin\Omega T + \frac{1}{\Omega^2}\left(-B_0+V_0-1\right)\left(\cos\Omega T-1\right), \qquad (8)$$

$$B(T)-B_0 = \frac{\Omega^2-1}{\Omega}U_0\sin\Omega T - \frac{\Omega^2-1}{\Omega^2}\left(-B_0+V_0-1\right)\left(\cos\Omega T-1\right). \qquad (9)$$

B_0 and V_0 on the right hand sides of (7)-(9) always appear in the combination $-B_0+V_0$, so smaller initial southerly winds (larger ageostrophic winds) are equivalent to larger positive initial buoyancies.

Larger N (larger Ω) reduces the $1/\Omega$ and $1/\Omega^2$ factors in (7) and (8) and thus appears to reduce jet wind strength (but there's more to the story).

Evolution of U, V, B with U_0 and B_0 set to 0

lat=35°N , N=0.01s^{-1}, V_0= (0.4, solid lines) or (0.8, dashed lines).

$\alpha = 0°$

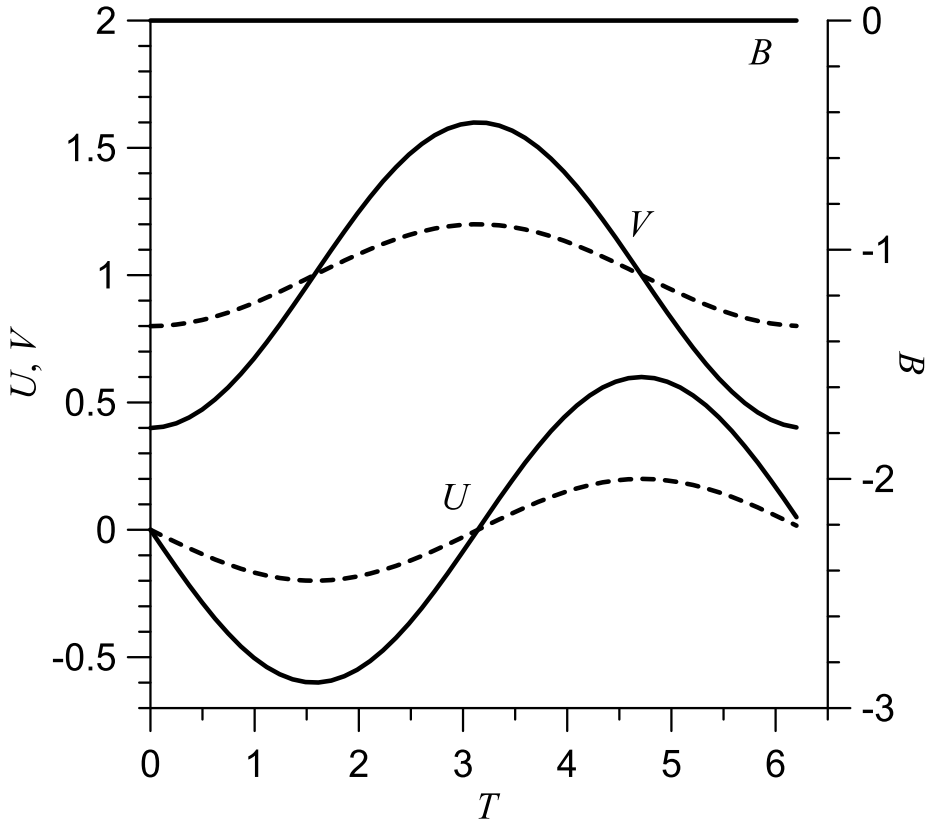

$\alpha = 1.0°$

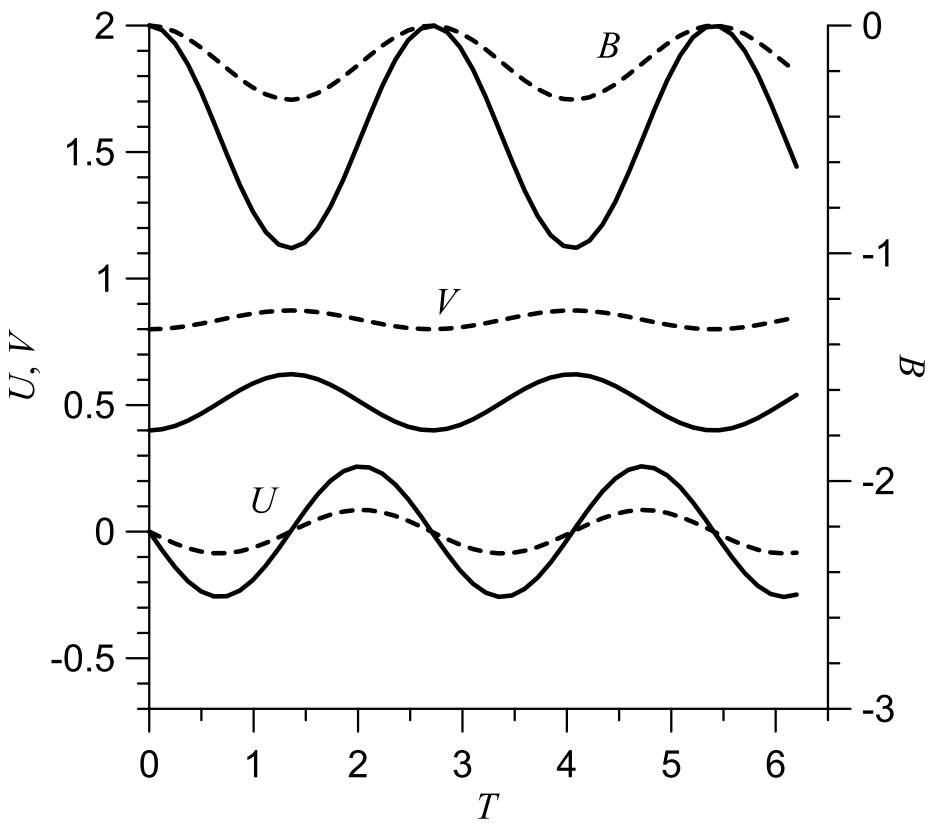

Peak jet winds weaken with slope angle. No strong jet...

Estimating appropriate B_0 for the Great Plains LLJ

(1) Adopt the notion of a residual layer (Stull 1988):

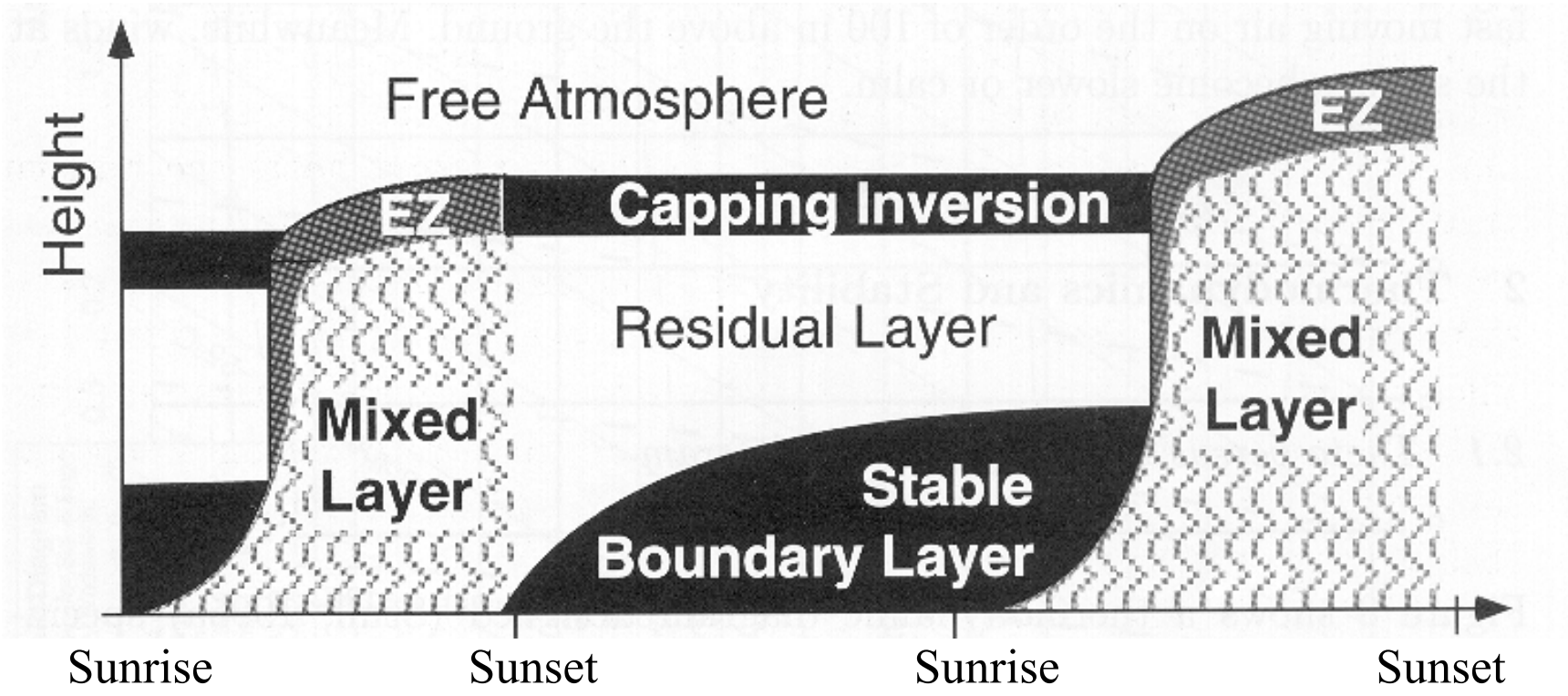

(2) Now tilt it -- so we have a "tilted residual layer" (TRL).

(3) See what can be inferred about B_0 from this TRL.

Anatomy of a tilted residual layer (TRL)

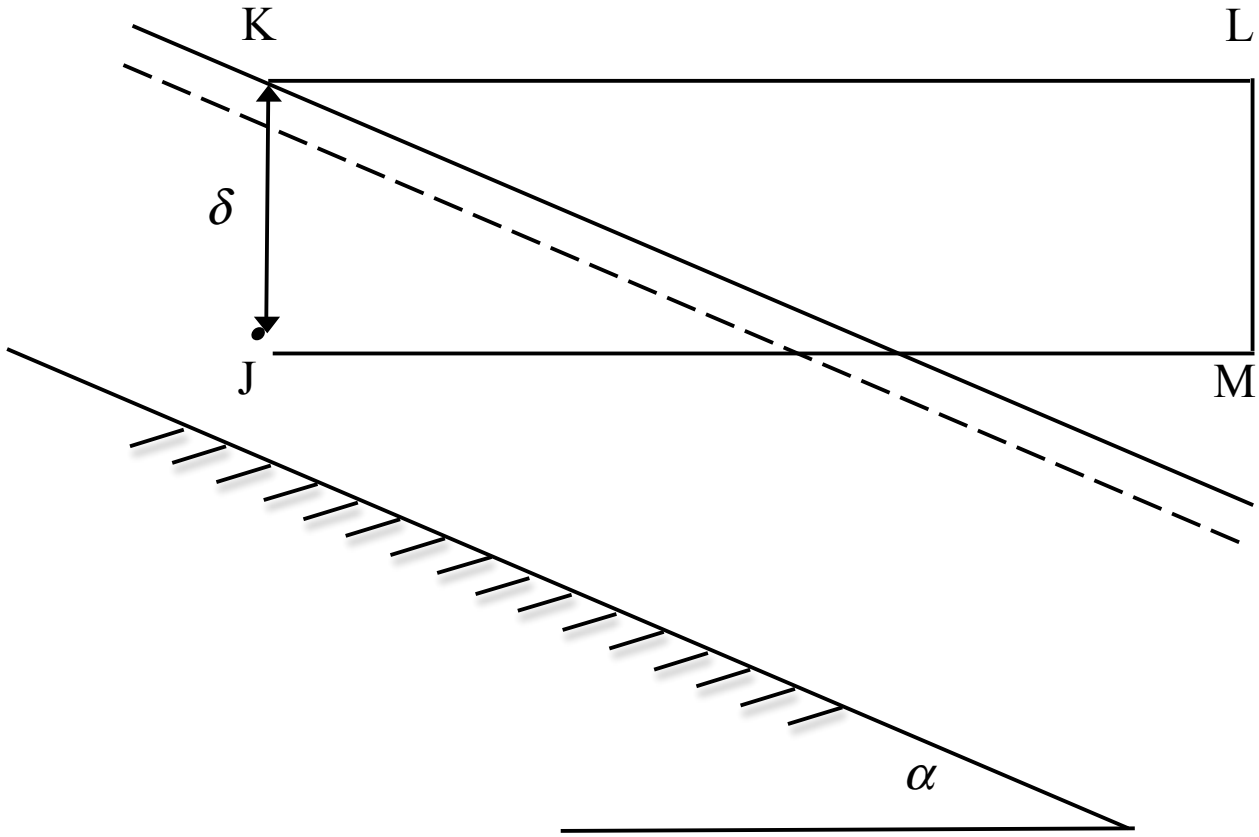

Dashed line is base of inversion. Sloping line through K is top of inversion. J is an air parcel. δ is distance of parcel from top of inversion. L is in free atmosphere at same elevation as K. M is in free atmosphere at same elevation as J. Horizontal line KL is an environmental isentrope.

Estimating B_0 in a TRL

θ is approximately constant (= θ_0) from J up to base of inversion, and then increases by $\Delta\theta$ across interface. So θ at K is $\theta_0 + \Delta\theta$.

Since KL is an environmental isentrope, θ at L is also $\theta_0 + \Delta\theta$.

$\theta \downarrow$ from L to M by an amount equal to the environmental potential temperature gradient $d\theta_e/dz$ times the altitude difference δ (> 0) between L and M. So θ at M is $\theta_0 + \Delta\theta - \delta\, d\theta_e/dz$.

Thus, the initial buoyancy for the parcel at J is $b_0 = N^2\delta - g\Delta\theta/\theta_r$, and the corresponding non-dimensional buoyancy is:

$$B_0 = \frac{N^2 \sin\alpha}{f v_G}\,\delta - \frac{\sin\alpha}{f v_G}\,\frac{g\Delta\theta}{\theta_r}. \qquad (10)$$

So larger stratification N is associated with larger B_0!

Implications of the B_0 formula

For values of the parameters typical of the Great Plains, B_0 is sensitive to all of the parameters in (10).

At locations slightly beneath the capping inversion, δ is small and (10) indicates parcels there have negative buoyancy.

For parcels at low levels (e.g., where LLJ occur), (10) indicates the buoyancy is positive. Also: larger N associated with larger B_0!

So, the TRL has a downward-directed initial buoyancy gradient, and therefore a means for a "jet-like" profile to evolve from a well-mixed (with respect to momentum and θ) initial state.

Peak LLJ wind speeds in the TRL model

Applying (10) in (8) at the time $T = \pi/\Omega$ when V attains a peak amplitude $V_{\max}$ (taking $U_0 = 0$) yields

$$V_{\max} = \frac{2f^2}{f^2+N^2\sin^2\alpha}\left(\frac{N^2\sin\alpha}{f v_G}\delta - \frac{\sin\alpha}{f v_G}\frac{g\Delta\theta}{\theta_r} + 1\right) + V_0\left(1 - \frac{2f^2}{f^2+N^2\sin^2\alpha}\right) \qquad (11)$$

Eq. (11) yields large $V_{\max}$ for parcels with small V_0 (large initial ageostrophic wind speed $1-V_0$) located at low levels (large δ) within a TRL with a weak capping inversion (small $\Delta\theta$).

V_{max} versus slope angle α for a parcel with V_0=0.4

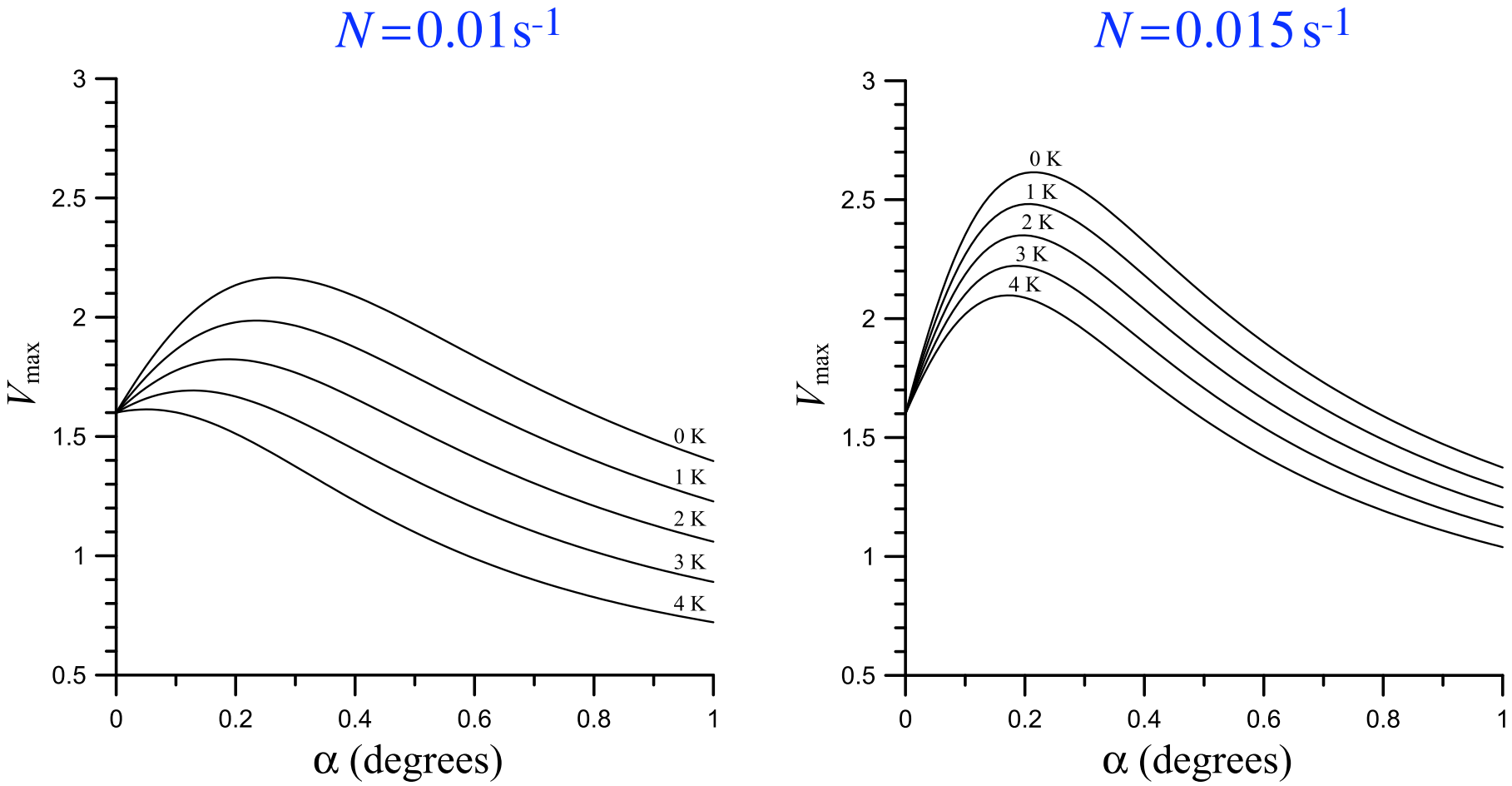

Parcel located 1000 m beneath a capping inversion. Results shown for five capping inversion strengths, $\Delta\theta = 0, 1, 2, 3, 4$ K.

V_{max} versus slope angle α for a parcel with V_0=0.8

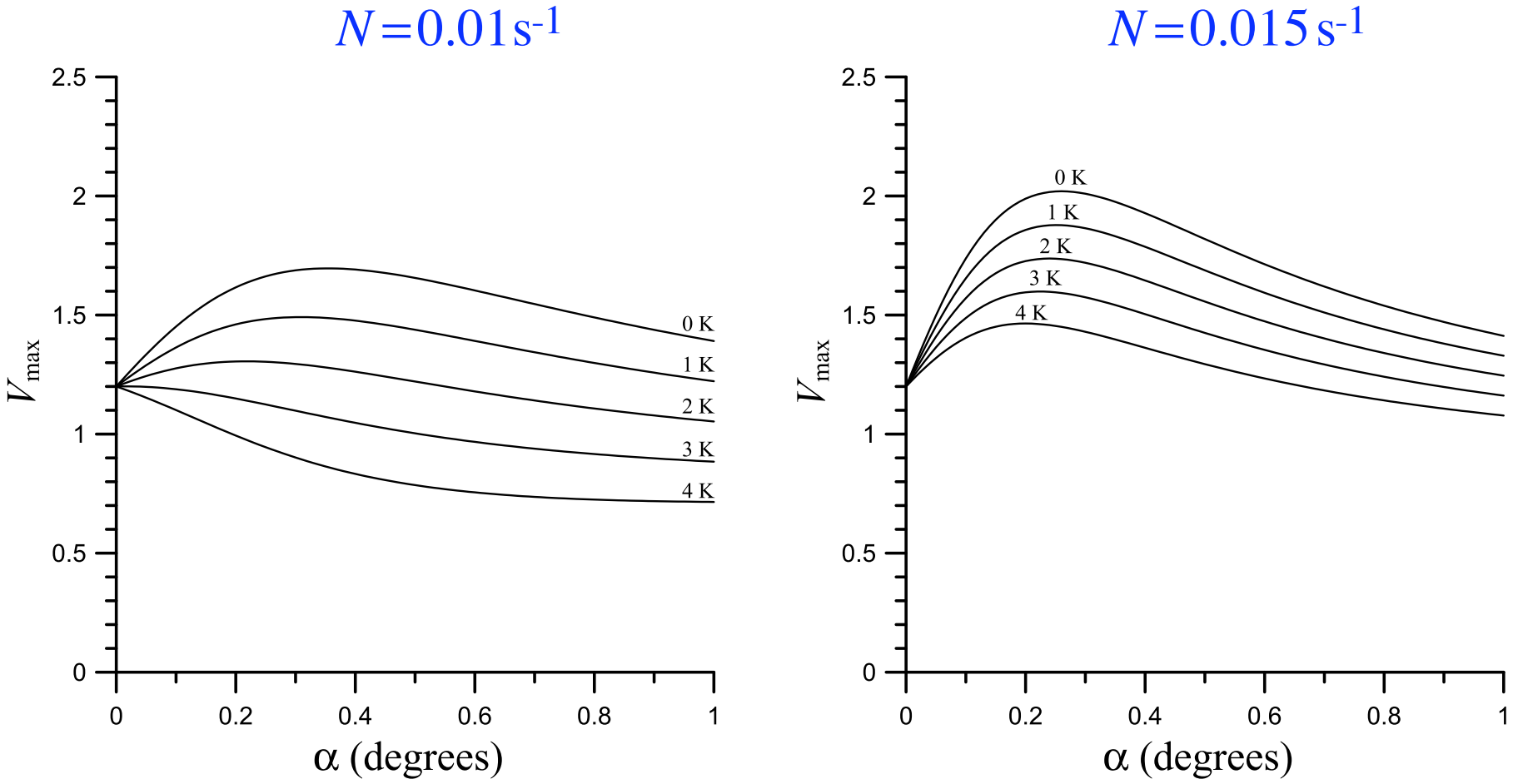

Parcel located 1000 m beneath a capping inversion. Results shown for five capping inversion strengths, $\Delta\theta$ = 0, 1, 2, 3, 4 K.

Optimum slope angle

The slope angle α^* at which $V_{\max}$ is largest is obtained from $(dV_{\max}/d\alpha)\big|_{\alpha=\alpha^*} = 0$ as

$$\alpha^* = -\frac{f v_G (1-V_0)}{N^2\delta - g\Delta\theta/\theta_r} + \sqrt{\left(\frac{f v_G (1-V_0)}{N^2\delta - g\Delta\theta/\theta_r}\right)^2 + \frac{f^2}{N^2}}. \qquad (12)$$

α^* is roughly in the 0.10°–0.20° range for V_0=0.4,

α^* is roughly in the 0.15°–0.25° range for V_0=0.8.

Terrain slope of Slapout is ≈0.15°.

Qualitatively good agreement with climatological studies (Bonner 1968; Walters et al. 2008).